Available online at www.sciencedirect.com

SciVerse ScienceDirect

journal homepage: www.elsevier.com/locate/he

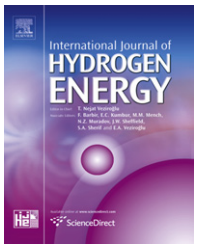

State-of-health diagnosis based on hamming neural network using output voltage pattern recognition for a PEM fuel cell

Jonghoon Kim [a,*], *Inhae Lee* [b], *Yongsug Tak* [b], *B.H. Cho* [a]

[a] *Power Electronics System Laboratory, School of Electrical Engineering and Computer Science, Seoul National University, San 56-1, Sillim-dong, Gwanak-ku, Seoul 151-744, Republic of Korea*

[b] *Materials and Electro-Chemistry Laboratory, Department of Chemical Engineering, Inha University, Incheon 402-751, Republic of Korea*

ARTICLE INFO

Article history:
Received 2 September 2011
Received in revised form
10 November 2011
Accepted 14 November 2011
Available online 17 December 2011

Keywords:
Polymer electrolyte membrane (PEM) fuel cell
Hamming neural network
State-of-health (SOH)
Pattern recognition

ABSTRACT

This work investigates a pattern recognition-based diagnosis approach as an application of the Hamming neural network to the identification of suitable fuel cell model parameters, which aim to diagnose state-of-health (SOH) for a polymer electrolyte membrane (PEM) fuel cell. The fuel cell output voltage (FCOV) patterns of the 20 PEM fuel cells were measured, together with the model parameters, as representative patterns. Through statistical analysis of the FCOV patterns for 20 single cells, the Hamming neural network is applied for identification of the representative FCOV pattern that matches most closely of the pattern of the arbitrary cell to be measured. Considering the equivalent circuit fuel cell model, the purpose is to select a representative loss ΔR_d, defined as the sum of two losses (activation and concentration losses). Consequently, the selected cell's ΔR_d is properly applied to diagnose SOH of an arbitrary cell through the comparison with those of fully fresh and aged cells with the minimum and maximum of the ΔR_d in experimental cell group, respectively. This avoids the need for repeated parameter measurement. Therefore, these results could lead to interesting perspectives for diagnostic fuel cell SOH.

1. Introduction

Fuel cell systems convert the "chemical" energy contained in many hydrogenous fuels into electrical and thermal energies. Fuel cells are widely considered as promising and environmentally friendly energy-conversion solutions for the future since they can offer high fuel economy, through high efficiency, and substantially lower CO_2 emissions [1–3]. Considering different fuel cell types that can be encountered, polymer electrolyte membrane (PEM) fuel cell are considered to be the most promising energy technology with the advantages of low-operating temperature, high current density, high potential for low cost and volume, fast start-up ability, and suitability for discontinuous operation become the most promising and attractive candidate for electric vehicle power [4–6]. However, fuel cells still suffer from a low reliability and a short lifetime, which make them difficult to satisfy user's requirements. Moreover, when dealing with reliability and durability, the fuel cell diagnosis has been identified among the critical issues that need to be developed to increase system performance. The development of diagnostic can help evaluating the fuel cell state-of-health (SOH) [7–10]. Precise SOH diagnosis is critical in practical applications where it is necessary to determine how long the fuel cell will last, and to minimize the risk of permanent internal damage.

In recent years, much research has been devoted to developing improved methods for SOH diagnosis. The behavior model-based methods [11–14] are fast to implement

* *Corresponding author*. Tel.: +82 2 880 1785; fax: +82 2 878 1452.
E-mail address: qwzxas@hanmail.net (J. Kim).

0360-3199/$ – see front matter
doi:10.1016/j.ijhydene.2011.11.092

and overcome the strong limitation of physical ones that use the mathematical equations describing the actual physical phenomena occurring in each fuel cell's components and which need an accurate identification of the PEM fuel cell inner parameters. Among those black-box models [15,16], many are based on fuzzy logic and neural network, which have many advantages. They can indeed learn and approximate any continuous nonlinear function and does not need the knowledge of the physical process behind it. However, they need good quality data, which means data describing the whole process to be modeled.

In general, fuel cell output voltage is highly dependent to the pulse current. The magnitude of the decrease in this voltage, called the voltage variance, is associated with changes in fuel cell model parameters that include open-circuit voltage (OCV; E_{Nernst}), three types of losses such as ohmic losses (R_{ohm}), activation losses (R_{act}) concentration losses (R_{conc}), and double layer capacitance (C_{dl}) [17–19]. Since these parameters vary with electrochemical characteristics [20,21], temperature [22–24], and aging effect [25–27], the voltage variance can be used to determine the magnitude of the parameters for the fuel cell model. Specifically, two losses, namely, the activation losses (R_{act}) and the concentration losses (R_{conc}), are considered as critical factors that determine the magnitudes of the voltage variance.

When a constant pulse current is commonly applied to the cells, the magnitudes of the respective voltage variances are different. In addition, the fuel cell output voltage (FCOV) pattern of each cell is almost constant under identical conditions such as pulse current magnitude and time interval. Therefore, the FCOV pattern can be used to discriminate among PEM fuel cells with different characteristics for improved SOH diagnosis. This investigation proposes the use of a Hamming neural network [28–33] for such FCOV pattern recognition. The Hamming neural network is generally used and designed explicitly for binary pattern recognition. In this work, the Hamming neural network is used to evaluate several predetermined representative FCOV pattern and determine the one that is closest to the input FCOV pattern by comparing the inner product. Through the statistical analysis, the proposed method can perform recognition of an arbitrary FCOV pattern. Representative FCOV patterns are collected from 20 single cells, together with four characteristic parameters for each cell. Considering the equivalent circuit fuel cell model, a representative loss $\Delta R_d(R_{act} + R_{conc})$ defined as the sum of two losses (activation and concentration losses) of the selected representative FCOV pattern is properly applied to diagnose SOH of an arbitrary cell through the comparison with those of fully fresh and aged cells with the minimum and maximum of the ΔR_d in experimental cell group, respectively. Consequently, these results enable us to provide interesting perspectives for diagnostic fuel cell SOH without the need for repeated parameter measurement.

The remainder of this work is organized as follows. The experimental setup for obtaining the representative FCOV patterns of the 20 PEM fuel cells is described in Section 2. Section 3 presents the basic principle of the Hamming neural network. In addition, the double layer charging effect of the PEM fuel cell for FCOV pattern implementation is presented in Section 4. A pattern recognition-based diagnosis approach as an application of the Hamming neural network, which aim to diagnose SOH is presented in detail in Section 5. In addition, few experimental results are reported to verify the proposed approach in the same section. The final section summarizes this work.

2. Experimental setup

The experimental setup was designed for obtaining the representative FCOVs of the 20 PEM fuel cells by the 'Materials and Electro-Chemistry Laboratory in Inha University'. A block diagram of the setup is presented in Fig. 1. All experiments were conducted using a subscale single cell (active area of 25 cm^2). The membrane electrode assembly (MEA) that used was a GORE™ PRIMEA® SERIES 57 MEA (W. L. Gore & Associates, Inc.) that has 0.4 mg/cm^2 Pt on both the anode and the cathode. The GDLs were SIGRACET® GDL 10 BB (thickness of 420 μm, SGL Carbon Japan Ltd.). High purity H_2 (99.99%) gas for the anode feed, high purity Air (O_2 21%/N_2) for the cathode feed, and high purity N_2 (99.99%) gas for both the anode and cathode feed were used. The pulse current profile was applied during the experiments in order to obtain the FCOV pattern. As a consequence, the gas flow rates of H_2 and O_2 corresponding to the pulse current were supplied (W^{in}_{an,H_2}, W^{in}_{ca,O_2}). These gases flows need to be controlled rapidly and efficiently in order to avoid hydrogen/oxygen starvation. These flows supplied to the anode and cathode should exceed the hydrogen/oxygen flows necessary for the reaction (W^{react}_{an,H_2}, W^{react}_{ca,O_2}). The hydrogen flow and oxygen flow that react to produce a certain cell current I, are defined as (1) and (2), respectively.

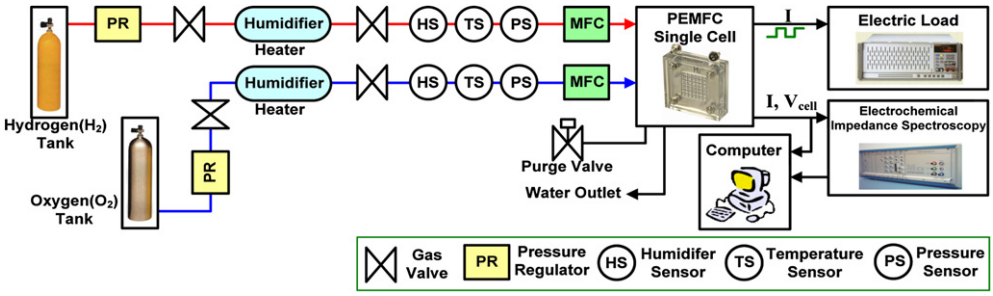

Fig. 1 – Experimental setup for measuring the fuel cell output voltage (FCOV) pattern for 20 polymer electrolyte membrane (PEM) fuel cells.

$$W_{an,H_2}^{react} = M_{H_2} \times \frac{I}{2F} \tag{1}$$

$$W_{ca,O_2}^{react} = M_{O_2} \times \frac{I}{4F} \tag{2}$$

where M_{H_2} and M_{O_2} are the hydrogen molar mass (2.016×10^{-3} kg/mol) and oxygen molar mass (32×10^{-3} kg/mol), respectively. This leads to hydrogen/oxygen excess ratios, λH_2 and λO_2, that are defined as the ratio of the supplied hydrogen/oxygen to the hydrogen/oxygen used in the anode and cathode, as expressed in (3) and (4), respectively.

$$\lambda_{H_2} = \frac{W_{an,H_2}^{in}}{W_{an,H_2}^{react}} \tag{3}$$

$$\lambda_{O_2} = \frac{W_{ca,O_2}^{in}}{W_{ca,O_2}^{react}} \tag{4}$$

It is necessary to determine the maximum hydrogen/oxygen excess ratios to avoid hydrogen/oxygen starvation. The experiments were performed with H_2 and O_2 under the constant stoichiometry mode of $\lambda H_2 = 1$ and $\lambda O_2 = 1.5$. The gas flow rates corresponding to a stoichiometry of 1 and 1.5 for H_2 and air are 150 ml/min and 488 ml/min with a constant pressure (101.325 kPa), respectively. These gases were humidified in a bubbling humidifier before entering the fuel cell. The temperature of the cell was 70 °C and the humidification temperature was 70 °C (100% RH).

3. Hamming neural network

The Hamming neural network [28–33] is used for pattern recognition, as shown in Fig. 2. It is one of the simplest examples of a competitive network and is designed explicitly to solve binary pattern recognition issues. The Hamming neural network decides which representative pattern is closest to the current pattern by comparing the inner products. Its objective is to decide which prototype vector is closest to the input vector. The Hamming neural network consists of two layers: the feedforward layer and the recurrent layer.

3.1. *Feedforward layer*

The feedforward layer calculates a correlation or inner product between each representative pattern and the current pattern in order to find the Hamming distance (HD) from calculation the difference between dimension m and HD. In order to calculate the inner products, weight matrix $\mathbf{W^1}$ is a set of prototype vectors and is transformed into the binary form, in addition to bias vector, $\mathbf{b^1}$, in (5) and (6), respectively.

$$\mathbf{W}^1 = \begin{bmatrix} {}_1\mathbf{w}^{iT} \\ {}_2\mathbf{w}^{iT} \\ \vdots \\ {}_S\mathbf{w}^{iT} \end{bmatrix} = \frac{1}{2}\begin{bmatrix} {}_1\mathbf{w}^1 & {}_2\mathbf{w}^1 & \cdots & {}_S\mathbf{w}^1 \\ {}_1\mathbf{w}^2 & {}_2\mathbf{w}^2 & \cdots & {}_S\mathbf{w}^2 \\ \vdots & \vdots & \ddots & \vdots \\ {}_1\mathbf{w}^R & {}_2\mathbf{w}^R & \cdots & {}_S\mathbf{w}^R \end{bmatrix} = \begin{bmatrix} \mathbf{p}_1^T \\ \mathbf{p}_2^T \\ \vdots \\ \mathbf{p}_S^T \end{bmatrix}, \tag{5}$$

$$\mathbf{b}^1 = [R, R, \cdots, R]^T = \left[\frac{m}{2}, \frac{m}{2}, \cdots, \frac{m}{2}\right]^T \tag{6}$$

where each row of $\mathbf{W^1}$ represents a prototype vector which it is required to be recognize, and each element of $\mathbf{b^1}$, $m/2$ is the threshold value and is set equal to the number of elements in each input vector R, S is the number of neurons. As expressed in (7), it is high desirable to have the ith ($1 \le 1 \le i \le R$) node in this layer compute $m - HD({}_i\mathbf{w},\mathbf{p})$ for a given input vector $\mathbf{p}$, where $HD({}_i\mathbf{w},\mathbf{p})$ is the Hamming distance between vectors ${}_i\mathbf{w}$ and $\mathbf{p}$. Then, the net input of node is as in (8), namely, the feedforward layer output. Finally, these outputs are equal to the inner (Eq. (9)). The neuron in this layer with the largest output corresponds to the prototype pattern that is closest in Hamming distance to the input pattern.

$$\mathbf{W}^1\mathbf{p} = [m - HD({}_i\mathbf{w}, \mathbf{p})] - HD({}_i\mathbf{w}, \mathbf{p}) \tag{7}$$

$$\mathrm{net}_i = \mathbf{n}^1 = \mathbf{W}^1\mathbf{p} + \frac{m}{2} = m - HD({}_i\mathbf{w}, \mathbf{p}) \quad i = 1, 2, \cdots, S \tag{8}$$

$$\mathbf{a}^1 = \mathbf{W}^1\mathbf{p} + \mathbf{b}^1 = \begin{bmatrix} \mathbf{p}_1^T\mathbf{p} + R \\ \mathbf{p}_2^T\mathbf{p} + R \\ \vdots \\ \mathbf{p}_S^T\mathbf{p} + R \end{bmatrix} = \mathbf{purelin}(\mathbf{W}^1\mathbf{p} + \mathbf{b}^1) \tag{9}$$

3.2. *Recurrent layer*

The recurrent layer is known as the MAXNET. It is a competitive layer that performs the winner-take-all (WTA) operation, whose purpose is to enhance the initial dominant response of the ith node and suppress the others [33]. As expressed in (10), the neurons are initialized with the outputs of the feedforward layer, which indicates the correlation between the prototype vectors and the input vector.

$$\mathbf{a}^2(0) = \mathbf{a}^1 \tag{10}$$

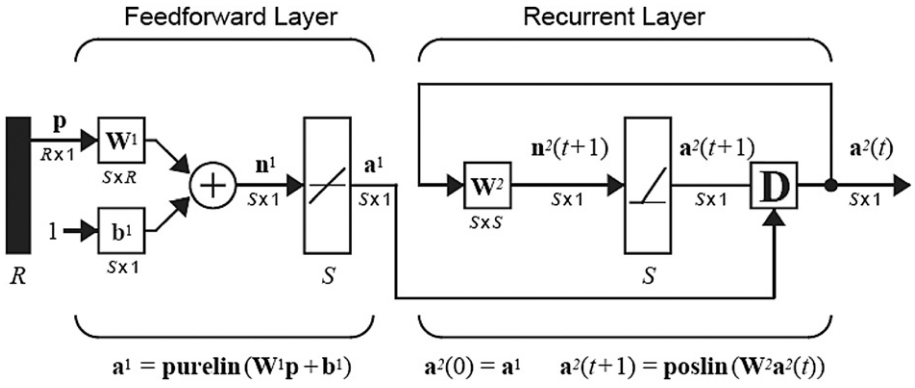

Fig. 2 – Hamming neural network.

As a result of recurrent processing, the ith node responds positively whereas the responses of all remaining nodes decay to zero. Thus, in order to determine a winner (which only has a positive output), the neurons compete with each other. Then, as expressed in (11), the recurrent layer output is updated according to the following recurrence relation using a positive transfer function (**poslin**):

$$\mathbf{a}^2(t+1) = \mathbf{poslin}\left(\mathbf{W}^2\mathbf{a}^2(t)\right) \tag{11}$$

This processing requires self-feedback connections and negative lateral inhibition connections in which the output of each neuron has an inhibitory effect on all of the other neurons [33]. The $n \times n$ weight matrix of the recurrent layer $\mathbf{W}^2$ is taken in (12). The weights in this layer are set so that the diagonal elements are 1, and the off-diagonal elements have a small negative value, where $0<\varepsilon < 1/(S-1)$ is called the lateral interaction coefficient. Thus, weight values of 1 and $-\varepsilon$ can be set for the appropriate elements of $\mathbf{W}^2$ in (13), where $1 \le i \le S$ and $1 \le j \le S$.

$$\mathbf{W}^2 = \begin{bmatrix} {}_1\mathbf{w}^1 & {}_1\mathbf{w}^2 & \cdots & {}_1\mathbf{w}^S \\ {}_2\mathbf{w}^1 & {}_2\mathbf{w}^2 & \cdots & {}_2\mathbf{w}^s \\ \vdots & \vdots & \ddots & \vdots \\ {}_i\mathbf{w}^1 & {}_i\mathbf{w}^2 & \cdots & {}_i\mathbf{w}^s \end{bmatrix} = \begin{bmatrix} 1 & -\varepsilon & \cdots & -\varepsilon \\ -\varepsilon & 1 & \cdots & -\varepsilon \\ \vdots & \vdots & \ddots & \vdots \\ -\varepsilon & -\varepsilon & \cdots & 1 \end{bmatrix} \tag{12}$$

$$\mathbf{a}_i^2(t+1) = \mathbf{poslin}\left(\mathbf{a}_i^2(t) - \varepsilon \sum_{j \ne i} \mathbf{a}_j^2(t)\right) \tag{13}$$

Each neuron's output decreases in proportion to the sum of the other neuron's outputs. The output of the neuron with the largest initial output decreases more slowly than the outputs of the other neurons. But eventually, only one neuron will have a positive output. The index of the recurrent layer neuron with a stable positive output is the index of the prototype vector that is the best match with the input.

3.3. *Competitive learning*

Learning is based on clustering of input data to group similar objects and separate dissimilar ones. It is assumed in this clustering technique that the number of classes is S, which is known a priori. The network to be trained for learning is WTA network or Kohonen network [33] and is shown in Fig. 3. The WTA network classifies input vectors into one of the specified S categories according to the clusters detected in the training set. The learning algorithm treats the set of S weight vectors as variable vectors that need to be learned. Prior to the learning, the normalization of all weight vectors is required. For example, considered WTA network without lateral inhibition as shown in Fig. 3(a), the WTA learning rule is described by

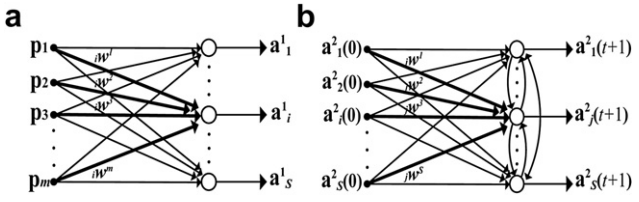

Fig. 3 – Winner-take-all (WTA) network. (a)Without lateral inhibition (feedforward layer), (b) With lateral inhibition (recurrent layer).

two-step computation, similarity matching and updating. As expressed in (14), the similarity matching finds the winner ${}_i\hat{\mathbf{w}}(q)$, which is the pattern closest to the current input pattern.

$$\|\mathbf{p}(q+1) - {}_i\hat{\mathbf{w}}(q)\| = \min_{1\le j\le S}\{\|\mathbf{p}(q+1) - {}_j\hat{\mathbf{w}}(q)\|\} \tag{14}$$

where, ${}_i\hat{\mathbf{w}}(q)$ denotes the normalized vector ${}_i\hat{\mathbf{w}}(q)$ at the qth time step, as expressed in (15).

$${}_i\hat{\mathbf{w}} = \frac{{}_i\mathbf{w}}{\|{}_i\mathbf{w}\|} \tag{15}$$

With the similarity matching, the weight vector lengths and directions should be identical and modified, respectively. Since a long weight vector could lead to a large output even if there were a large angle between the weight vector and input. Therefore, the weight normalization should be needed and required to renormalize the winning node's weight vector ${}_i\hat{\mathbf{w}}(q)$ at each iteration. After the winning neuron has been identified and declared a winner, its weight must be adjusted so that the distance $\|\mathbf{p}(q+1) - {}_i\hat{\mathbf{w}}(q)\|$, namely S is reduced in the current time step, preferable along the gradient in the weight space ${}_i\hat{\mathbf{w}}^1, {}_i\hat{\mathbf{w}}^2, \cdots, {}_i\hat{\mathbf{w}}^m$. It seems reasonable to reward the weights of the winning neuron with an increment of weight in the negative gradient direction $\|\mathbf{p}(q+1) - {}_i\hat{\mathbf{w}}(q)\|$. After all, the purpose of this weight updating is to produce the new normalized vector ${}_i\hat{\mathbf{w}}(q+1)$ from the previous normalized vector ${}_i\hat{\mathbf{w}}(q)$, as expressed in (16).

$$\begin{aligned} {}_i\hat{\mathbf{w}}(q+1) &= {}_i\hat{\mathbf{w}}(q) + \alpha(q+1)(\mathbf{p}(q+1) - {}_i\hat{\mathbf{w}}(q)) \\ &= (1-\alpha(q+1)){}_i\hat{\mathbf{w}}(q) + \alpha(q+1)\mathbf{p}(q+1){}_j\hat{\mathbf{w}}(q+1) \\ &= {}_j\hat{\mathbf{w}}(q) \;\; for \;\; j = 1,2,\cdots,S; \;\; j \ne 1 \end{aligned} \tag{16}$$

$$\begin{aligned} \arg\min_j \|\mathbf{p} - {}_j\hat{\mathbf{w}}\| &= \arg\min_j (\mathbf{p} - {}_j\hat{\mathbf{w}})^T(\mathbf{p} - {}_j\hat{\mathbf{w}}) \\ &= \arg\min_j (\mathbf{p}^T\mathbf{p} + {}_j\hat{\mathbf{w}}^T{}_j\hat{\mathbf{w}} - 2\mathbf{p}^T{}_j\hat{\mathbf{w}}) \\ &= \arg\max_j (\mathbf{p}^T{}_j\hat{\mathbf{w}}) = \arg\max_j ({}_j\hat{\mathbf{w}}^T\mathbf{p}) \end{aligned} \tag{17}$$

where, $\alpha(q+1)$ is a suitable learning constant at the $(q+1)^{\text{th}}$ time step. As a consequence, using the equality, it can be inferred that searching for the minimum of S distance corresponds to finding the maximum among the S scalar products in (17). The ith competing neuron wins if it has the largest net input $({}_i\hat{\mathbf{w}}^T\mathbf{p})$, that is, if the input pattern $\mathbf{p}$ correlates maximally with ${}_i\hat{\mathbf{w}}$. As expected in (18), the net input net_i of each neuron i is proportional to the angle between $\mathbf{p}$ and the prototype vector.

$$\text{net}_i = \mathbf{a}_i^1 = {}_i\hat{\mathbf{w}}^T\mathbf{p} = \|{}_i\hat{\mathbf{w}}\|\|\mathbf{p}\|\cos({}_i\hat{\mathbf{w}}, \mathbf{p}) \tag{18}$$

where, $\cos({}_i\hat{\mathbf{w}}, \mathbf{p})$ is angle θ_i between the two vectors ${}_i\hat{\mathbf{w}}$ and $\mathbf{p}$. This implies that the ith node wins if the input pattern is more parallel to its weight vector ${}_i\hat{\mathbf{w}}$ than to any other ${}_j\hat{\mathbf{w}}$, $j \ne i$. Fig. 4 shows a simple graphical representation of the competitive learning. Especially, as shown in Fig. 4(c), after competitive learning, the final weight vectors point to the centers of gravity of classes.

4. Double layer charging effect of the PEM fuel cell

The equivalent electrical circuit for the charge double layer effect on the cell voltage is shown in Fig. 5. In this figure, C_{dl} is

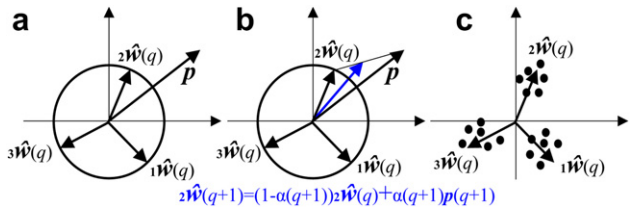

Fig. 4 – Competitive learning. (a)Winner weight $_2\hat{w}(q)$, (b) Updating the weight of the winner neuron, (c) Final weight vectors.

the equivalent capacitance depending on the charge double layer. Since the electrodes of a PEM fuel cell are porous, the capacitance C_{dl} is very large and can be in the order of several Farads [34]. R_{ohm}, R_{act}, and R_{conc} are equivalent resistances to the ohmic, activation, and concentration overvoltages, respectively [17–19]. V_{Cdl} is the overvoltage due to the common effects of the double capacitive layer, the activation, and the concentration resistances. The double capacitive layer overvoltage follows the first-order dynamic given in (19).

$$V_{Cdl} = \left(I_{FC} - C_{dl}\frac{dV_{Cdl}}{dt}\right)(R_{act} + R_{conc}) \tag{19}$$

In the equivalent circuit in Fig. 5, there is a first-order delay in the activation and the concentration voltage components (resistance R_{act} and R_{conc}). This delay is caused by the double layer charging effect considered as one important electrochemical phenomenon linking the cell voltage to load current variations. This effect appears at both electrodes, but is far more important at the cathode [35]. Two electrodes are separated by a solid membrane that allows only the H^+ ions flow, but blocks electron flow. Therefore, the electrons flow form the anode through the external load and gather at the cathode, to which hydrogen protons are attracted at the same time [35]. Two opposite charged layers are then formed across the porous boundary between the cathode and the membrane. The charge double layer is partly due to diffusion effects, and also due to the reaction between the electrons in the electrodes and the ions in the electrolyte. When there is an increase (decrease) in the fuel cell current, there is a delay until the fuel cell voltage decreases (increases). The ohmic overpotential is not affected by the double layer charging effect as it is directly related to the current (resistance R_{ohm}).

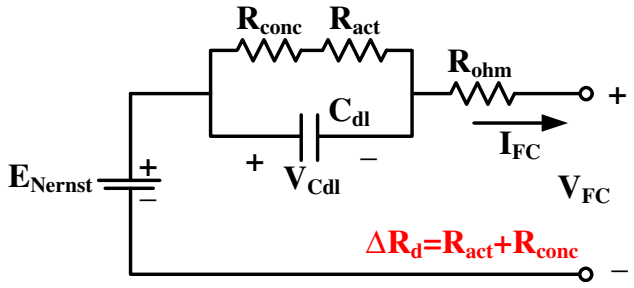

Fig. 5 – Fuel cell equivalent circuit model: open-circuit voltage (OCV; E_{Nernst}), ohmic losses (R_{ohm}), activation losses (R_{act}), and concentration losses (R_{conc}), and double layer capacitance (C_{dl}).

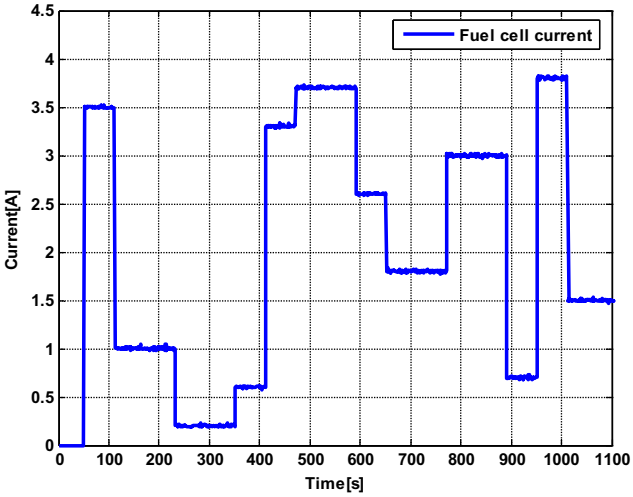

Fig. 6 – Pulse current profile covering currents from 0A to 3.8A for obtaining the FCOV pattern (1100s).

On the equivalent circuit of Fig. 5, the capacitance is positioned in parallel with the activation and concentration voltages to take into account the dynamic effect of these voltage drops. This resulting loop is then connected in a series with the Nernst potential and with the ohmic voltage drop. The dynamic equation of the model presented in Fig. 5 is represented by

$$\frac{dV_{Cdl}}{dt} = \frac{1}{C_{dl}}I_{FC} - \frac{1}{\tau}V_{Cdl} \tag{20}$$

where τ is the fuel cell electrical time-constant [36] defined as

$$\tau = (R_{act} + R_{conc}) \cdot C_{dl} = \left(\frac{V_{act} + V_{conc}}{I_{FC}}\right) \cdot C_{dl} \tag{21}$$

Including the dynamic behavior represented [16], the resulting fuel cell voltage is defined as

$$V_{FC} = E_{Nernst} - V_{ohm} - V_{Cdl} \tag{22}$$

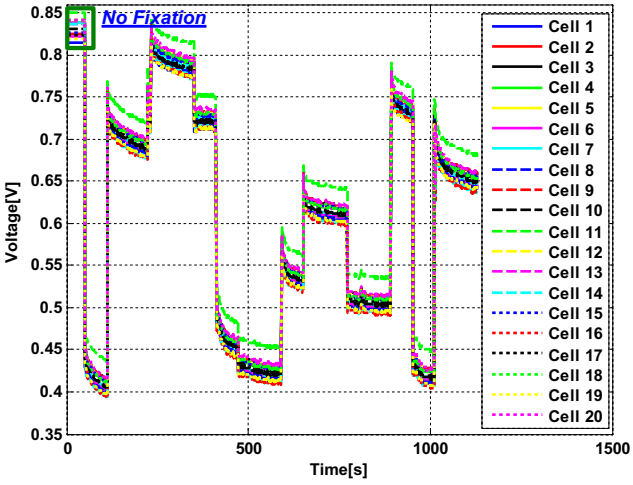

Fig. 7 – Unfixed fuel cell output voltage (FCOV) patterns for 20 single cells.

Table 1 – Initial starting points of each fuel cell output voltage (FCOV) pattern for 20 polymer electrolyte membrane (PEM) fuel cells [V].

Cell	OCV[V]	Cell	OCV[V]	Cell	OCV[V]	Cell	OCV[V]
No.1	0.814	No.6	0.822	No.11	0.850	No.16	0.842
No.2	0.825	No.7	0.839	No.12	0.839	No.17	0.824
No.3	0.839	No.8	0.837	No.13	0.839	No.18	0.842
No.4	0.839	No.9	0.839	No.14	0.837	No.19	0.819
No.5	0.822	No.10	0.831	No.15	0.827	No.20	0.842

The transient performance of the fuel cell equivalent circuit model over short or long time period is differently observed [18]. In this work, however, it can be assumed that the fuel cell current has a step or a similar shape for a short or long time. In such cases, the V_{Cdl} is calculated as in equation (19), and the voltage approximates to equation (23) after some time passes unless the current level changes significantly. Then, the sum of two resistances R_{act} and R_{conc} is defined as the magnitude of the ΔR_d in (24).

$$V_{Cdl} \approx I_{FC} \cdot (R_{act} + R_{conc}) \tag{23}$$

$$\Delta R_d = R_{act} + R_{conc} \tag{24}$$

The ΔR_d among the PEM fuel cells is frequently varied with electrochemical characteristics, temperature, and aging effect. As a result, the ΔR_d can be considered as an important factor to determine the PEM fuel cell SOH.

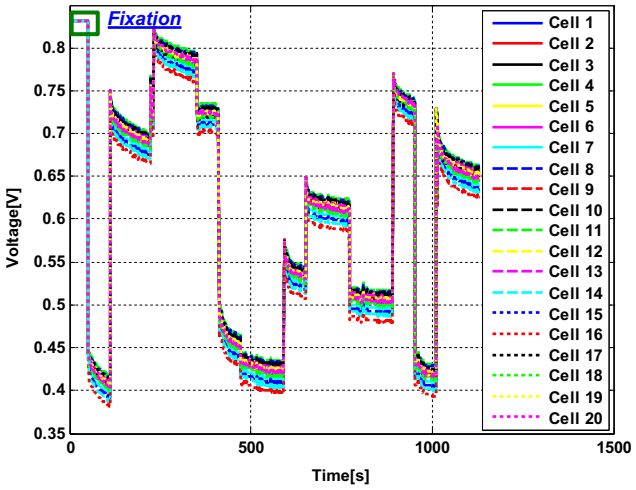

Fig. 9 – Fixed fuel cell output voltage (FCOV) patterns for 20 single cells.

5. Pattern recognition-based diagnosis approach

5.1. *Fuel cell output voltage (FCOV) pattern*

The pulse current profile covering currents from 0 A to 3.8 A is applied to the fuel cell about 1100 s, as shown in Fig. 6. Then, for a pulse current profile, the fuel cell output voltage (FCOV) data collected is shown in Fig. 7. This figure enables us to show the

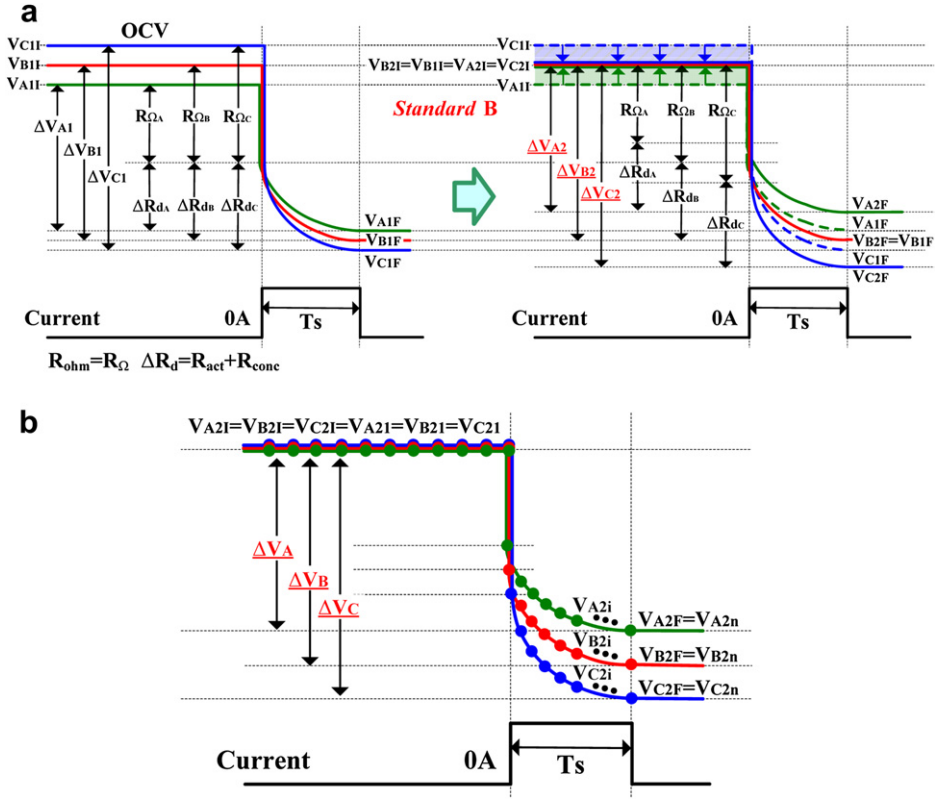

Fig. 8 – A method to recognize the fuel cell output voltage (FCOV) pattern through statistical analysis. (a) Initial starting voltage points (ISVP) fixation, (b) Each FCOV pattern comparison after ISVP.

Table 2 – Characteristics of AVE and STD in relation to voltage variance.

Voltage variance	AVE	STD
Large voltage variance	Small	Large
Small voltage variance	Large	Small

transient behaviors of the PEM fuel cell over a long time period. It is observed that as the load current is reduced, the output voltage increases to a certain value, but from there, it reaches to its final state. On the other hand, when the load current is increased, the output voltage drops to a certain value, and again takes to reach to its final value. According to the transient behaviors over a long time period, the time-constant τ can be defined as 25 s for obtaining the ΔR_d in Section 5.4.

The FCOV pattern is recognized through experiments for 20 PEM fuel cells. For recognition of the FCOV pattern with the Hamming neural network, statistical analysis is absolutely necessary. Then, the initial starting points of each FCOV pattern should be fixed. However, as shown in Fig. 7 and Table 1, the initial starting voltage points (ISVP) of the 20 PEM fuel cells were not fixed due to their different electrochemical characteristics. Hence, the average and standard deviation of the 20 collected output voltages cannot be compared. Therefore, it is required to set a standard ISVP, as shown in Fig. 8(a). For example, consider three cells (A–C) with different ISVPs (VA1I–VC1I). If the standard fuel cell is set as B (VB1I = VB2I), then the voltages of A and C are higher and lower, respectively (VA1I⇒VA2I, VC1I⇒VC2I). Therefore, the three ISVPs are fixed at one point, as shown in Fig. 8(b). Based on this rule, the average and standard deviation of voltage A can be expressed in (25) and (26), respectively. In addition, the average (AVE) and standard deviation (STD) of three cells can be compared in (27) and (28), respectively.

$$\text{Fuel cell}(\text{A})_{\text{AVE}} = \frac{\sum_{i=1}^{n} V_{\text{A2i}}}{n} \quad (n = 1, 2, \cdots, \text{F}) \tag{25}$$

$$\text{Fuel cell}(\text{A})_{\text{STD}} = \sqrt{\frac{\sum_{i=1}^{n} \left(V_{\text{A2i}} - \text{Fuel cell}(\text{A})_{\text{AVE}}\right)^2}{n}} \quad (n = 1, 2, \cdots, \text{F}) \tag{26}$$

$$\text{Fuel cell}(\text{A})_{\text{AVE}} > \text{Fuel cell}(\text{B})_{\text{AVE}} > \text{Fuel cell}(\text{C})_{\text{AVE}} \tag{27}$$

$$\text{Fuel cell}(\text{A})_{\text{STD}} < \text{Fuel cell}(\text{B})_{\text{STD}} < \text{Fuel cell}(\text{C})_{\text{STD}} \tag{28}$$

The fixed FCOV patterns are given in Fig. 9. These results enable us to obtain the fixed ISVP (0.831 V) among 20 PEM fuel cells. All averages and standard deviations for the collected FCOV patterns can be compared through statistical analysis.

Table 3 – Four characteristic parameters for learning by the Hamming neural network.

SVP	C1	Standard deviation of the FCOV
AVP(f)	C2	Average of the FCOV (f)
SVP(f)	C3	Standard deviation of the FCOV (f)
MVP(f)	C4	Minimum of the FCOV (f)

Standard: Cell No.10; (f): fixation (ISVP).

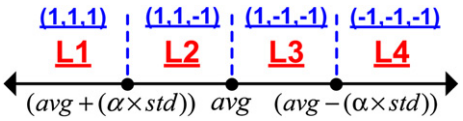

Fig. 10 – Four levels as to three standards.

The average (AVE) and standard deviation (STD) in relation to voltage variance are presented in Table 2. Specifically, the STD values increased at large voltage variance. These features of AVE and STD are used to implement some characteristic parameters of the Hamming neural network, as shown in Table 3.

5.2. *Characteristic parameters of the FCOV pattern*

As indicated in Table 3, characteristic parameters C1–C4 are learned by the Hamming neural network using the average, standard deviation, and minimum of the FCOV patterns. Each value of the four characteristic parameters corresponding to the 20 representative FCOV patterns is transformed into 1 and −1 element array with four levels, as shown in Fig. 10. If these patterns are not transformed into this binary form of same norm, the pattern recognition performance can be distorted by the one parameter of C1–C4, which has the large real value. In Fig. 10, *avg* is the average and *std* is the standard deviation of each characteristic parameter. These values are given in Table 4. The levels of each parameter are decided by three standard, viz., $avg - (\alpha \times std)$, *avg*, and $avg + (\alpha \times std)$. The levels are decided according to the values of the parameter, as shown in Fig. 11. For example, if the value is larger than $avg - (\alpha \times std)$ and smaller than *avg*, the level is L3, and if the

Table 4 – Average (*avg*) and standard deviation (*std*) of each characteristic parameters (C1–C4).

Cell	SVP	AVP(f)	SVP(f)	MVP(f)
No.1	0.135255	0.613936	0.135255	0.414
No.2	0.136703	0.608087	0.136703	0.407
No.3	0.135834	0.606375	0.135834	0.406
No.4	0.137067	0.603357	0.137067	0.402
No.5	0.135398	0.612046	0.135398	0.412
No.6	0.135542	0.610155	0.135542	0.410
No.7	0.137514	0.597681	0.137514	0.396
No.8	0.137819	0.593896	0.137819	0.392
No.9	0.135835	0.606375	0.135835	0.406
No.10	0.135983	0.604484	0.135983	0.404
No.11	0.135044	0.616772	0.135044	0.417
No.12	0.136921	0.605249	0.136921	0.404
No.13	0.136994	0.604303	0.136994	0.403
No.14	0.138102	0.590095	0.138102	0.388
No.15	0.135184	0.614881	0.135184	0.415
No.16	0.138604	0.584436	0.138604	0.382
No.17	0.135327	0.612991	0.135327	0.413
No.18	0.137215	0.601465	0.137215	0.400
No.19	0.135688	0.608265	0.135688	0.408
No.20	0.136848	0.606195	0.136848	0.405
Average (avg)	0.136444	0.605052	0.136444	0.404200
Standard (std)	0.001702	0.008333	0.001702	0.009099

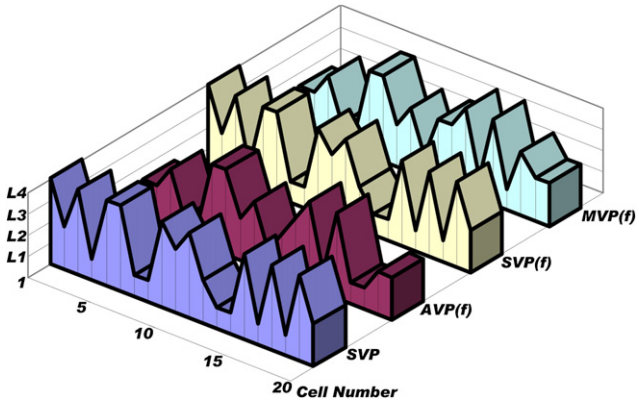

Fig. 11 – Characteristics of four representative patterns.

value is larger than *avg* and smaller than $avg + (\alpha \times std)$, the level is L2. α is a tuning value and chosen as 0.5 to make the characteristic differences of 20 representative patterns.

5.3. *Pattern recognition with the Hamming neural network*

As shown in Fig. 12, the feedforward layer calculates the inner product between each representative pattern and the current pattern. As expresses in (29) and (30), the value of each of the four characteristic parameters corresponding to 20 representative patterns is transformed into the binary from and stored in the weight matrix $\mathbf{W}^1$.

$$\mathbf{W}^1 = \begin{bmatrix} {}_1\mathbf{w}^{iT} \\ {}_2\mathbf{w}^{iT} \\ \vdots \\ {}_{20}\mathbf{w}^{iT} \end{bmatrix} = \frac{1}{2}\begin{bmatrix} {}_1\mathbf{w}^1 & {}_2\mathbf{w}^1 & \cdots & {}_{20}\mathbf{w}^1 \\ {}_1\mathbf{w}^2 & {}_2\mathbf{w}^2 & \cdots & {}_{20}\mathbf{w}^2 \\ \vdots & \vdots & \ddots & \vdots \\ {}_1\mathbf{w}^{12} & {}_2\mathbf{w}^{12} & \cdots & {}_{20}\mathbf{w}^{12} \end{bmatrix} = \begin{bmatrix} \mathbf{p}_1^T \\ \mathbf{p}_2^T \\ \vdots \\ \mathbf{p}_{20}^T \end{bmatrix} \tag{29}$$

$$\mathbf{b}^1 = [12, 12, \cdots, 12] \tag{30}$$

For a given input vector $\mathbf{p}$, the node in the feedforward layer generates the following output (31).

$$\mathbf{a}^1 = \mathbf{W}^1\mathbf{p} + \mathbf{b}^1 = \begin{bmatrix} \mathbf{p}_1^T\mathbf{p}+12 \\ \mathbf{p}_2^T\mathbf{p}+12 \\ \vdots \\ \mathbf{p}_{20}^T\mathbf{p}+12 \end{bmatrix} = \mathbf{purelin}(\mathbf{W}^1\mathbf{p} + 12) \tag{31}$$

The 20 neurons storing the results of the inner product in the feedforward layer compete with each other to determine a winner. Then, self-feedback connection and negative lateral inhibition connection are required to implement the WTA. As expressed in (32), the weights in the recurrent layer $\mathbf{W}^2$ are set so that the diagonal elements are 1, and the off-diagonal elements have a small negative value, where $0<\varepsilon < 1/(20-1)$ is called the lateral interaction coefficient ($\varepsilon = 0.01$). After the competition in (33), only one neuron will have a nonzero output, and this neuron indicates the representative pattern that is closest to a current pattern.

$$\mathbf{W}^2 = \begin{bmatrix} {}_1\mathbf{w}^1 & {}_1\mathbf{w}^2 & \cdots & {}_1\mathbf{w}^{20} \\ {}_2\mathbf{w}^1 & {}_2\mathbf{w}^2 & \cdots & {}_2\mathbf{w}^{20} \\ \vdots & \vdots & \ddots & \vdots \\ {}_i\mathbf{w}^1 & {}_i\mathbf{w}^2 & \cdots & {}_i\mathbf{w}^{20} \end{bmatrix} = \begin{bmatrix} 1 & -0.01 & \cdots & -0.01 \\ -0.01 & 1 & \cdots & -0.01 \\ \vdots & \vdots & \ddots & \vdots \\ -0.01 & -0.01 & \cdots & 1 \end{bmatrix} \tag{32}$$

$$\mathbf{a}_i^2(t+1) = \mathbf{poslin}\left(\mathbf{a}_i^2(t) - 0.01\sum_{j\neq i}\mathbf{a}_j^2(t)\right) \tag{33}$$

5.4. *Verification*

Based on the time-constant defined as $\tau = (R_{act} + R_{conc})\cdot C_{dl}$, Representative loss ΔR_d results for 20 single cells were previously measured after 25 s with the pulse current, and compared with those of arbitrary cells, as listed in Table 5. When the pulse current profile shown in Fig. 6 is applied to two arbitrary cells, the outputs of the two layers of the Hamming neural network for two arbitrary cells are shown in Fig. 13. In each case, we see that in the recurrent layer, only the selected representative FCOV pattern has a nonzero output. As shown in Fig. 13(a), a representative loss ΔR_d of an arbitrary cell 1 (0.0106 Ω) is similar with to that of the selected representative FCOV pattern (No.8; 0.0108 Ω). In addition, the FCOV pattern of the No.17 (0.0056 Ω) is selected as the representative FCOV pattern that is closest to the current FCOV pattern of an arbitrary cell 2 (0.0055 Ω), as shown in Fig. 13(b).

5.5. *SOH diagnosis*

The representative loss ΔR_d of the selected FCOV pattern in Section 5.4 is properly applied to diagnose SOH of an arbitrary cell through the comparison with those of fully fresh and aged cells with the minimum and maximum of the ΔR_d in experimental cell group, respectively. As expressed in (34), the SOH of an arbitrary cell can be diagnosed using the selected cell pattern's ΔR_d, $\Delta R_d^{selected}$.

$$\underset{arbitrary}{SOH} = \left|\frac{\Delta R_d^{selected} - \Delta R_d^{aged}}{\Delta R_d^{fresh} - \Delta R_d^{aged}}\right| \tag{34}$$

where, ΔR_d^{fresh} (No.11; 0.0044 Ω) and ΔR_d^{aged} (No.16; 0.0133 Ω) are each ΔR_d values of fully fresh and aged cells among 20 single cells. The fully fresh cell has the largest SOH (SOH = 1), on the

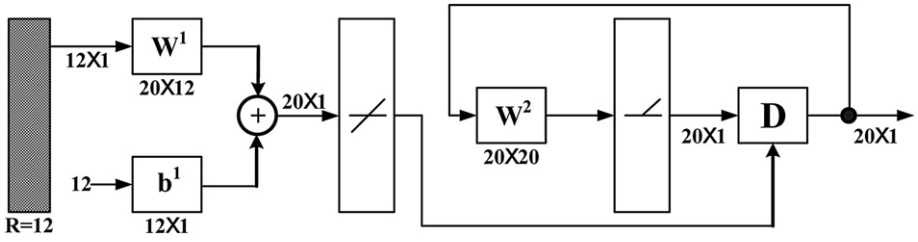

Fig. 12 – Hamming neural network in this work.

Table 5 – Representative loss $\Delta R_d(R_{act} + R_{conc})$ results for 20 single cells after 25 s by the time-constant $\tau = (R_{act} + R_{conc}) \cdot C_{dl}[\Omega]$.

Cell	$\Delta R_d[\Omega]$	Cell	$\Delta R_d[\Omega]$	Cell	$\Delta R_d[\Omega]$	Cell	$\Delta R_d[\Omega]$
No.1	0.0052	No.6	0.0062	No.11	0.0044	No.16	0.0133
No.2	0.0070	No.7	0.0097	No.12	0.0078	No.17	0.0056
No.3	0.0073	No.8	0.0108	No.13	0.0080	No.18	0.0087
No.4	0.0083	No.9	0.0072	No.14	0.0117	No.19	0.0066
No.5	0.0058	No.10	0.0076	No.15	0.0049	No.20	0.0074

other hand, the fully aged cell has the smallest SOH (SOH = 0). 20 experimental single cells have each ΔR_d within this range of 0.0044–0.0133 Ω. With obtained ΔR_d values (0.0108 Ω and 0.0056 Ω) of two arbitrary cells, the diagnosed SOHs of two arbitrary cells are expressed in (35) and (36), respectively. (SOH range: 0–1).

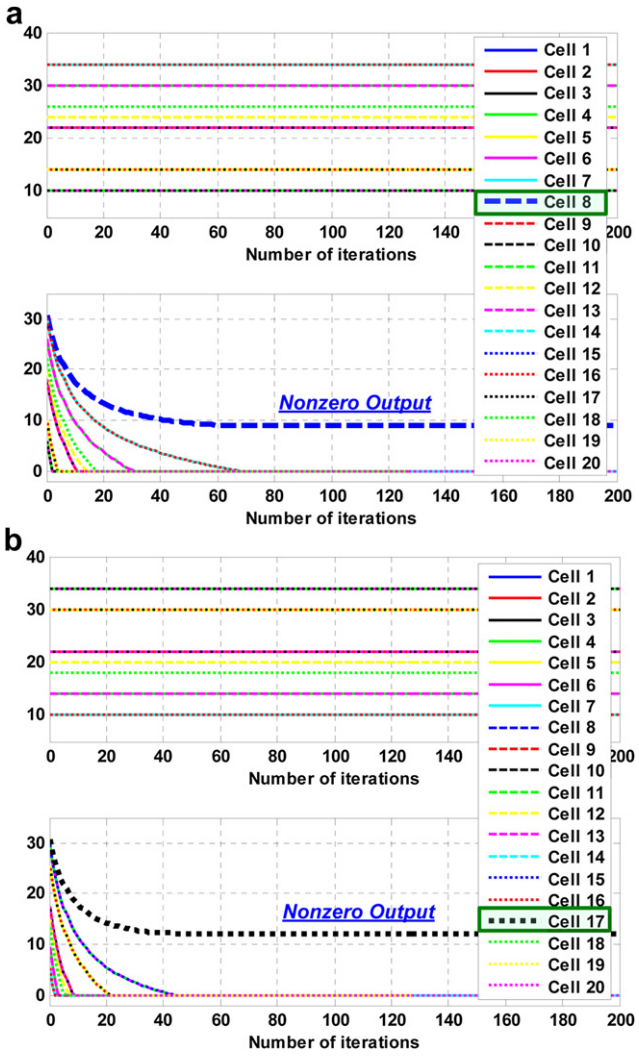

Fig. 13 – Outputs of two layers by the Hamming neural network. (a) Arbitrary cell 1, selected fuel cell output voltage (FCOV) pattern : No.8, (b) Arbitrary cell 2, selected fuel cell output voltage (FCOV) pattern : No.17.

$$\underset{\text{arbitrary1}}{SOH} = \left|\frac{\Delta R_d^{selected} - \Delta R_d^{aged}}{\Delta R_d^{fresh} - \Delta R_d^{aged}}\right| = \left|\frac{0.0108 - 0.0133}{0.0044 - 0.0133}\right| \approx 0.2809 \quad (35)$$

$$\underset{\text{arbitrary2}}{SOH} = \left|\frac{\Delta R_d^{selected} - \Delta R_d^{aged}}{\Delta R_d^{fresh} - \Delta R_d^{aged}}\right| = \left|\frac{0.0056 - 0.0133}{0.0044 - 0.0133}\right| \approx 0.8651 \quad (36)$$

We can see, the range of SOH is from 0 to 1, and 1 means the cell is totally healthy, or it is new, and 0 means the cell cannot meet the power demand of the practical applications. These results enable to us to provide interesting perspectives for diagnostic fuel cell SOH without the need for repeated parameter measurement of an arbitrary cell. For reference, it is assumed that R_{ohm} is constant (0.0955 Ω) due to little difference in electrochemical characteristics compared with that of the ΔR_d among the cells.

6. Conclusion

Precise SOH diagnosis is critical in practical applications where it is necessary to determine how long the fuel cell will last, and to minimize the risk of permanent internal damage. Therefore, a method to diagnose SOH for a PEM fuel cell, using a pattern recognition based approach as an application of the Hamming neural network to the identification of suitable fuel cell model parameters, has been presented in this work. Through statistical analysis of the FCOV patterns for 20 single cells, the Hamming neural network is applied for identification of the representative FCOV pattern that matches most closely of the pattern of the arbitrary cell to be measured. The selected cell's ΔR_d is properly applied to diagnose SOH of an arbitrary cell through the comparison with those of fully fresh and aged cells with the minimum and maximum of ΔR_d in experimental cell group, respectively. This avoids the need for repeated parameter measurement of an arbitrary cell. Therefore, these results could lead to interesting perspectives for diagnostic fuel cell SOH.

The other purpose of the proposed approach is to discriminate the cells that have similar electrochemical characteristics among the cells, is called the screening process. Through screening process, the cells that have similar electrochemical characteristics are finally selected, and can be used for stable configuration of a stack that consists of multiple cells in series. There is no determined minimal number of cells to be considered for stable configuration of a stack. Consequently, considered in screening process, the equivalent circuit model of the stack can be simplified as that of a unit cell, irrespective of number of unit cells.

Acknowledgment

This work was supported by the New and Renewable Energy Program of the Korea Institute of Energy Technology Evaluation and Planning (KETEP) grant funded by the Korea government Ministry of Knowledge Economy (No. 20104010100490).

REFERENCES

[1] Sun H, Zhang G, Guo L, Liu HA. Study of dynamic characteristics of PEM fuel cells by measuring local currents. Int J Hydrogen Energy 2009;34:5529–36.
[2] Yousfi-Steiner N, Hissel D, Moçotéguy Ph, Candusso D. Non intrusive diagnosis of polymer electrolyte fuel cells by wavelet packet transform. Int J Hydrogen Energy 2011;36:740–6.
[3] Asghari S, Mokmeli A, Samavati M. Study of PEM fuel cell performance by electrochemical impedance spectroscopy. Int J Hydrogen Energy 2010;35:9283–90.
[4] Corbo P, Migliardini F, Veneri O. PEFC stacks as power sources for hybrid propulsion systems. Int J Hydrogen Energy 2009;34:4635–44.
[5] Kovacevic G, Tenconi A, Bojoi R. Advanced DC-DC converter for power conditioning in hydrogen fuel cell systems. Int J Hydrogen Energy 2008;33:3215–9.
[6] Chen P-C. Output-feedback voltage tracking control for input-constrained PEM fuel cell systems. Int J Hydrogen Energy 2011;36:14608–21.
[7] Kurz T, Hakenjos A, Krämer J, Zedda M, Agert C. An impedance-based predictive control strategy for the state-of-health of PEM fuel cell stacks. J Power Sources 2008;180:742–7.
[8] Fouquet N, Doulet C, Nouillant C, Dauphin-Tanguy G, Ould-Bouamama B. Model based PEM fuel cell state-of-health monitoring via ac impedance measurements. J Power Sources 2006;159:905–13.
[9] Onanena R, Oukhellou L, Candusso D, Same A, Hissel D, Aknin P. Estimation of fuel cell operating time for predictive maintenance strategies. Int J Hydrogen Energy 2010;35:8022–9.
[10] Onanena R, Oukhellou L, Candusso D, Harel F, Hissel D, Aknin P. Fuel cells static dynamic characterizations as tools for the estimation of their ageing time. Int J Hydrogen Energy 2011;36:1730–9.
[11] Escobet T, Feroldi D, de Lira S, Puig V, Quevedo J, Riera J, et al. Model-based fault diagnosis in PEM fuel cell systems. J Power Sources 2009;192:216–23.
[12] Yuan X, Wang H, Colin Sun J, Zhang J. AC impedance technique in PEM fuel cell diagnosis – a review. Int J Hydrogen Energy 2007;32:4365–80.
[13] Rubio MA, Urquia A, Dormido S. Diagnosis of performance degradation phenomena in PEM fuel cells. Int J Hydrogen Energy 2010;35:2586–90.
[14] Hernandez A, Hissel D, Outbib R. Modeling and fault diagnosis of a Polymer Electrolyte Fuel Cell using electrical equivalent analysis. IEEE Trans Energy Convers 2010;25(1):148–60.
[15] Hissel D, Péra M-C, Kauffmann J-M. Diagnosis of automotive fuel cell power generators. J Power Sources 2004;128:239–46.
[16] Nitsche C, Schroedl S, Weiss W, Pucher E. Rapid (practical) methodology for creation of fuel cell systems models with scalable complexity. J Power Sources 2005;145:383–91.
[17] Corrêa JM, Farret A, Popov VA, Simões MG. Sensitivity analysis of the modeling parameters used in simulation of proton exchange membrane fuel cells. IEEE Trans Energy Convers 2005;20(1):211–8.
[18] Puranik SV, Keyhani Ali, Khorrami F. State-space modeling of proton exchange membrane fuel cell. IEEE Trans Energy Convers 2010;25(3):804–13.
[19] Adzakpa KP, Agbossou K, Dubé Y, Dostie M, Fournier M, Poulin A, et al. PEM fuel cells modeling and analysis through current and voltage transient behaviors. IEEE Trans Energy Convers 2008;23(2):581–91.
[20] Khajeh-Hosseini-Dalasm N, Ahadian S, Fushinobu K, Okazaki K, Kawazoe Y. Prediction and analysis of the cathode catalyst layer performance of proton exchange membrane fuel cells using artificial neural network and statistical methods. J Power Sources 2011;196:3750–6.
[21] Dhirde AM, Dale NV, Salehfar H, Mann MD, Han T-H. Equivalent electrical circuit modeling and performance analysis of a PEM fuel cell stack using impedance spectroscopy. IEEE Trans Energy Convers 2010;25(3):778–86.
[22] Shamardian O, Chertovich A, Kulikovsky AA, Khokhlov AR. A simple model of a high temperature PEM fuel cell. Int J Hydrogen Energy 2010;35:9954–62.
[23] Pfeifer P, Wall C, Jensen O, Hahn H, Fichtner M. Thermal coupling of a high temperature PEM fuel cell with a complex hydride tank. Int J Hydrogen Energy 2009;34:3457–66.
[24] Correa G, Borello F, Santarelli M. Sensitivity analysis of temperature uncertainty in an aircraft PEM fuel cell. Int J Hydrogen Energy 2011;36:14745–58.
[25] Ashraf Khorasani MR, Asghari S, Mokmeli A, Shahsamandi MH. Faghih Imani. A diagnosis method for identification of the detected cell(s) in the PEM fuel cells. Int J Hydrogen Energy 2010;35:9269–75.
[26] Weng F-B, Hsu C-Y, Li C-W. Experimental investigation of PEM fuel cell aging under current cycling segmented fuel cell. Int J Hydrogen Energy 2010;35:3664–75.
[27] Zhang S, Yuan X, Wang H, Mérida W, Zhu H, Shen J, et al. A review of accelerated stress tests of MEA durability in PEM fuel cells. Int J Hydrogen Energy 2009;34:388–404.
[28] Koutroumbas K, Kalouptsidis N. Generalized Hamming networks and applications. Neural Networks 2005;18(7):896–913.
[29] Chen L, Tokuda N, Nagaim A. Capacity analysis for a two-level decoupled Hamming network for associative memory under a noisy environment. Neural Networks 2007;20(5):598–609.
[30] Meilijon I, Ruppin E, Sipper M. A single-iteration threshold Hamming network. IEEE Trans Neural Net 1995;6(1):261–6.
[31] Sum JPF, Leung C-S, Tam PKS, Young GH, Kan WK, Chan L-W. Analysis for a class of winner-take-all model. IEEE Trans Neural Net 1999;10(1):64–71.
[32] Koutroumbas K, Kalouptsidis N. Qualitative analysis of the parallel and asynchronous modes of the Hamming network. IEEE Trans Neural Net 1994;5(3):380–91.
[33] Hagan MT, Demuth HB, Beale MH. Neural network design. 1st ed. Boston MA: PWS Publishing Co; 1995.
[34] Iqbal MT. Simulation of a small wind fuel cell hybrid energy system. Renew Energy 2003;28(4):511–22.
[35] Wang C, Hashem Nehrir M, Shaw SR. Dynamic models and model validation for PEM fuel cells using electrical circuits. IEEE Trans Energy Convers 2005;20(2):442–51.
[36] Gao F, Blunier B, Simões MG, Miraoui A. PEM fuel cell stack modeling for real-time emulation in hardware-in-the-loop applications. IEEE Trans Energy Convers 2011;26(1):184–94.